Reduction of ultrasonic pad stress and aluminum splash in copper ball bonding

A. Shah [a,*], A. Rezvani [a], M. Mayer [a], Y. Zhou [a], J. Persic [b], J.T. Moon [c]

[a] *Microjoining Laboratory, University of Waterloo, Waterloo, ON, Canada*
[b] *Microbonds Inc., Markham, ON, Canada*
[c] *MK Electron Co. Ltd., Yongin, Canada*

ARTICLE INFO

ABSTRACT

Given the cost and performance advantages associated with Cu wire, it is being increasingly seen as a candidate to replace Au wire for making interconnections in first level microelectronics packaging. A Cu ball bonding process is optimized with reduced pad stress and splash, using a 25.4 μm diameter Cu wire. For ball bonds made with conventionally optimized bond force and ultrasonic settings, the shear strength is ≈140 MPa. The amount of splash extruding out of bonded ball interface is between 10 and 12 μm. It can be reduced to 3–7 μm if accepting a shear strength reduction to 50–70 MPa. For excessive ultrasonic settings, elliptical shaped Cu bonded balls are observed, with the minor axis of the ellipse in the ultrasonic direction and the major axis perpendicular to the ultrasonic direction. To quantify the direct effect of bond force and ultrasound settings on pad stress, test pads with piezoresistive microsensors integrated next to the pad and the real-time ultrasonic force signals are used. By using a lower value of bond force combined with a reduced ultrasound level, the pad stress can be reduced by 30% while achieving an average shear strength of at least 120 MPa. These process settings also aid in reducing the amount of splash by 4.3 μm.

© 2010 Elsevier Ltd. All rights reserved.

1. Introduction

Thermosonic Au wire bonding is the most common first level interconnection technology used in microelectronics [1–3]. It is used to weld microwires to metallized pads of integrated circuits. In the microelectronics industry, there is a continuous push towards higher performance and lower costs [1–4]. This has led to an increased interest towards the development of lower-cost bonding wire materials. Compared to Au wire, Cu wire has lower cost, superior electrical and thermal conductivities, and higher mechanical strength [5–8]. However, since Cu is harder than Au, higher normal and ultrasonic forces are often used, resulting in bonds stronger than Au [9]. This results in ≈30% higher stress [10,11] delivered to the bond pad during Cu ball bonding than during Au ball bonding. The higher pad stress increases the likelihood of underpad damage, such as pad peeling [12,13] or bulk silicon cratering [9,14–16], particularly in the case of sensitive substrates, such as chips with low-*k* dielectrics.

Another effect of high bonding stress specifically observed during ball bonding of Cu on Al bond pad is the squeezing of Al pad metal from the peripheries of the ball bond [17–19]. The Al material squeezing (or splash) occurs in the ultrasonic direction. Splash is not desired as it results in localized pad thinning [19], which can reduce bond reliability.

There are several different approaches in reducing underpad stress and therefore limiting underpad damage during thermosonic bonding with Cu wire, e.g., by using softer Cu wire types [10,11], producing softer free air balls (FABs) [16–23], optimizing the bonding parameters [11,24,25], using higher frequency ultrasound (US) transducers [26], modifying the bond pad thickness and design [26,27], using harder bond pads, such as Ni/Pd, Ni/Au, and Ni/Pd/Au [27], or by using pre-US (ultrasound applied during impact portion of bonding) [28].

Previous studies reported that a double stage bonding process [24,25], in which an impact force (IF) that is higher than the bond force (BF) is used, aids in minimizing chip damage. Recently, a new fast method to reduce the extra stress observed during Cu ball bonding was reported [11]. It was found that an US level, about 15% lower than the conventionally optimized level can be used to obtain Cu ball bonds of comparable geometry and strength to that of Au ball bonds, while reducing the stress gap by ≈40%. The study considered the optimization of the US parameter only. The effect of BF on bonding quality and pad stress was not investigated. The present work addresses the question: what is the synergistic effect of BF and US on the bonding quality, splash, and the stress delivered to the bond pad? Parts of this work have been presented in [29]. Splash measurements and further discussions are added.

---

* Corresponding author.
  E-mail address: ashah011@engmail.uwaterloo.ca (A. Shah).

Nomenclature

B	minimum US level required for bonding, i.e. a US level lower than B results in ball NSOP
BDC	bonded ball diameter measured at capillary imprint
BDI	bonded ball diameter at interface
BDI_x	interfacial diameter of the elliptical bonded ball measured along the major axis
BDI_y	interfacial diameter of the elliptical bonded ball measured along the minor axis [BDI_y = BDI]
BF	bond force
BH	bonded ball height
C	conventionally optimized process window
D	maximum US level without UED
EFO	electrical flame-off
FAB	free-air ball

F_{US}	in situ ultrasonic force
F_{max}	maximum value of F_{US}
IF	impact force
NSOP	non-stick on pad
R	low-stress process window
S_i	interfacial area of the elliptical bonded ball
SDI	splash diameter at interface
SF	shear force
SS	shear strength
UED	ultrasonic enhanced deformation
US	ultrasound

2. Experimental

Thermosonic ball-wedge bonding is performed using a 25 μm diameter Cu wire (MK Electron Co. Ltd., Yongin, Korea) on an automatic ESEC 3100 ball-wedge bonder (Besi Esec, Cham, Switzerland), having an ultrasonic frequency of 128 kHz. The bonding is performed at a nominal heater plate temperature of 150 °C, resulting in a temperature of ≈138 °C at the bond pad. A commercial ceramics bottleneck capillary having a hole diameter of 35 μm and a chamfer diameter of 51 μm is used. During the formation of FABs, a homogeneous mixture of 95% nitrogen and 5% hydrogen is used as a shielding gas to prevent the oxidation of the molten FAB metal during solidification. The flow rate of the shielding gas is set to 0.48 l/min.

Two types of chips are used for wire bonding. Chip A [30] is a commercial wire bonding test chip available from Besi Esec (Cham, Switzerland), which provides bonding pads of various sizes but does not have any higher level integrated circuitry elements. Chip B [10,11] is a custom made microsensor test chip with integrated logic allowing for multiple sensing functions, produced using the 0.7 μm CMOS process of AMI Semiconductor (Oudenaarde, Belgium). Chip A is used for ball bond process optimization, which is aimed at obtaining maximum bond strength while controlling the bonded ball geometry (diameter and height). It is used to find the optimum levels of the process parameters (ultrasound, bond force, etc.) that result in maximum bond strength for the targeted bonded ball geometry. Chip B is used to measure the real-time pad stress acting at the bond pad during bonding.

The bond pad on Chip A consists of a 2 μm thick Al metallization layer over a polysilicon layer, which is deposited on the bulk Si. The polysilicon layer provides excellent adhesion between the Al layer and the bulk Si. The bond pad on Chip B consists of two separate layers of Al metallization (1 μm and 0.5 μm thick) over a layer of SiO$_2$ (≈1.5 μm thick), which is deposited on the bulk Si. Two layers of Ti diffusion barrier (each ≈0.25 μm thick) are sandwiched between the Al metal layers and the Al–SiO$_2$ layers, respectively, to prevent the diffusion of Al into SiO$_2$. The composition of the pad metal is similar on both the chips.

2.1. Optimization of processes

Ball bonding processes are optimized for eight levels of BF using a procedure similar to that reported in [10,11]. The procedure consists of four steps: (i) crescent bond optimization; (ii) FAB optimization; (iii) ball bond IF optimization; and (iv) ball bond US optimization. Each of these steps are described below.

The crescent bond parameters shown in Table 1 are found using an iterative optimization method [31]. These parameters result in symmetrical bonds with consistent wire tail length (length of the wire tail below the capillary tip), without any signs of fish tailing. The unit% is used for the ultrasonic parameter. It is proportional to the ultrasonic vibration amplitude where 1% is equivalent to a peak to peak amplitude of 26.6 nm measured at the center of the transducer tip.

The next step is to optimize the parameters of the electrical flame-off (EFO) process to obtain a 50 μm diameter FAB. FABs are made with four different levels of EFO current (10 FABs for each current level) while fixing all other parameters, including tail length to 500 μm, EFO time to 0.4 ms, and electrode to wire distance to 300 μm. The FAB diameters are measured using an optical microscope and fitted with a quadratic polynomial against the EFO current. From the fitted curve, the EFO current corresponding to a 50 μm FAB is determined. An example plot visualizing this procedure is shown in Fig. 1 from which the EFO current to obtain a 50 μm FAB is determined and is 82.5 mA. Using this current, sample FABs are made and the diameters are verified to be 50 ± 0.3 μm. A SEM micrograph of a typical 50 μm diameter FAB is shown in Fig. 2.

Next, the value of IF for the ball bond process is optimized so as to obtain the targeted ball geometry measured using an optical microscope: bonded ball diameter measured at the capillary imprint (BDC) of ≈58 μm and bonded ball height (BH) of ≈15 μm. These target values of BDC and BH are selected to meet the requirements for bonding on a 70 μm diameter bond pad with 120 μm bond pad pitch. To this end, sample ball bonds are made for different values of IF ranging between 1000 mN and 1300 mN. The BF and US values are kept constant at 400 mN and 52%, respectively. The selected US level is the minimum required US for bond formation for the given BF, and are taken from an earlier study [10,11]. Thus, there is no additional US effect on ball geometry. The optimum value of impact force is found to be 1200 mN. This value results in ball bonds with BDC = 58.2 ± 0.4 μm and BH = 14.2 ± 0.3 μm.

Table 1
Crescent bond parameters.

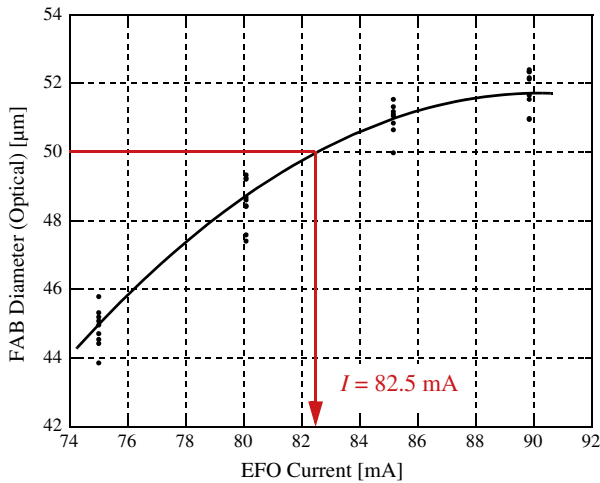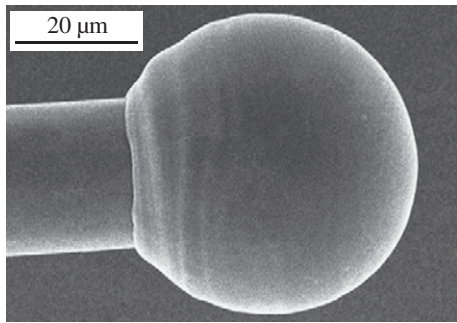|	
Impact force [mN]	800
Bond force [mN]	500
Bond time [ms]	75
Ultrasound [%]	65
Pre-ultrasound, off at impact [%]	30

Fig. 1. FAB diameter vs. EFO current.

Fig. 2. SEM micrograph of a typical 50 μm diameter FAB. Current = 82.5 mA, firing time = 0.4 ms.
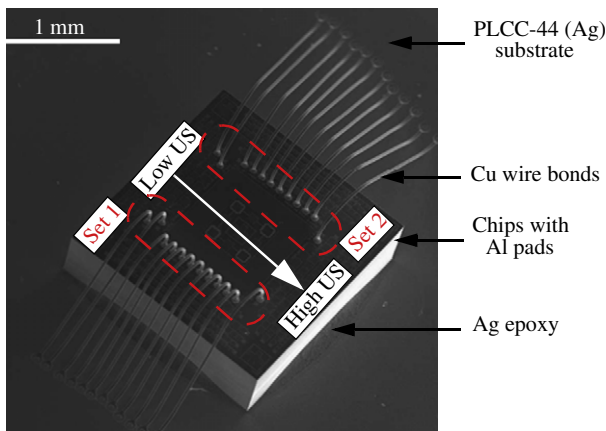

Fig. 3. SEM micrograph of the chip used for ball bonding process optimization (Chip A).

Ball bonding is performed on 10 wire bonding test chips (Chip A) at levels of BF: 100, 200, 300, 400, 500, 600, 700, and 800 mN. For each level of BF, ball bonding is performed by varying US from the minimum level required for bonding, B, in steps beyond a level D above which the ball experiences additional plastic deformation by US. The bonding time is fixed at 25 ms. A SEM micrograph of a typical bonded chip is shown in Fig. 3. On each chip, two identical sets of bonds are made (Fig. 3), where each set corresponds to the US levels from B to D for the given BF level. Bonding is repeated on

10 chips, resulting in a sample of 20 bonds for each US/BF combination. Due to the limitations of resources, the sample size used in the present study is lower than that typically used in the industry. In the future, a larger sample size can be used to obtain results with greater accuracy.

The balls are sheared using a standard shear tester and the shear force (SF) is measured. The shear strength (SS) of the ball bond is calculated as SF divided by the cross-sectional area A, where $A = \pi(BDC/2)^2$. The variations in BDC and SS as a function of US for each of the levels of BF are shown in Figs. 4 and 5, respectively. Each BDC measurement is the average of the bonded ball diameters in x- and y-directions at the capillary imprint as shown in Fig. 9b. For US levels lower than B, ball non-stick on pad (NSOP) is observed. The value of B is defined as the lowest US level where no NSOP is observed. The optimum US levels are selected at the transition point D. Beyond the level D, for any additional increase in the value of US, a sharp increase in BDC is observed. Since this additional deformation of the bonded ball is caused primarily due to US, it is called *ultrasound enhanced deformation* (UED) [32,33]. The value of D is defined as the maximum US level at which there is no UED. Table 2 summarizes the observed values of B and D for different levels of BF.

The SS results (Fig. 5) show that a maximum average shear strength of at least 130 MPa is obtained for each of the BF levels confirming the large size of the BF process window that is predicted by theory [35]. The maximum shear strength is observed for US levels close to level D. It is found that with increasing BF, the value of optimum US parameter D decreases. However, for lower BF levels, the window between B and D is found to be wider than that for high BF levels. Thus, according to [11], significantly lower levels of BF and US can be used to obtain Cu ball bonds with relatively high SS. This leads to a reduction in the pad stress during bonding, thereby reducing the chances of damage to the Si chip.

2.2. Splash

Fig. 6a and b shows the optical and SEM micrographs of typical pads, respectively, after the Cu ball bonds were sheared. Bright coloured Al splash material is visible outside the bond interface and is largest in the US direction. Within the bright splash, a dark ring is observed. Optical profilometry shows that the ring is $\approx$0.5–1 μm higher than the unbonded pad surface, and $\approx$2 μm lower than the maximum splash height that occurs at the edge. These observations and the SEM micrograph in Fig. 6b confirm that the ring constitutes part of the splash itself, and is outside the bond interface. The Al extruded can follow the shape of the ball (ball bulge) to a certain distance before extruding further out as shown by the illustration in Fig. 7. The Al extruded under the ball bulge can have a slope steep enough so the vertical illumination light is reflected out of the microscope resulting in the dark appearance (black ring).

The ball diameter at interface (BDI) and splash diameter at interface (SDI) are measured in US direction using an optical microscope as shown in Fig. 6a. The results are shown in Fig. 8. It is observed that the BDI decreases with increasing US levels. Higher US levels cause excessive ball deformation at the capillary contact, resulting in higher BDC and lower BDI. An example micrograph showing one of the smallest BDI samples is shown in Fig. 9a. The bonded ball deforms plastically in a similar way as a dough ball between two pressing plates under parallel movements oscillating in opposed directions. This analogous process forms the dough into a cylinder (noodle) ready for further processing into, e.g., a brezel or a baguette. The cylinder extends perpendicular to the oscillation direction. The higher the oscillation amplitude, the more pronounced the "noodle effect". In a similar way, the BDI decreases with increasing US. The reduction in the BDI is accompanied by a reduction in the circularity of the
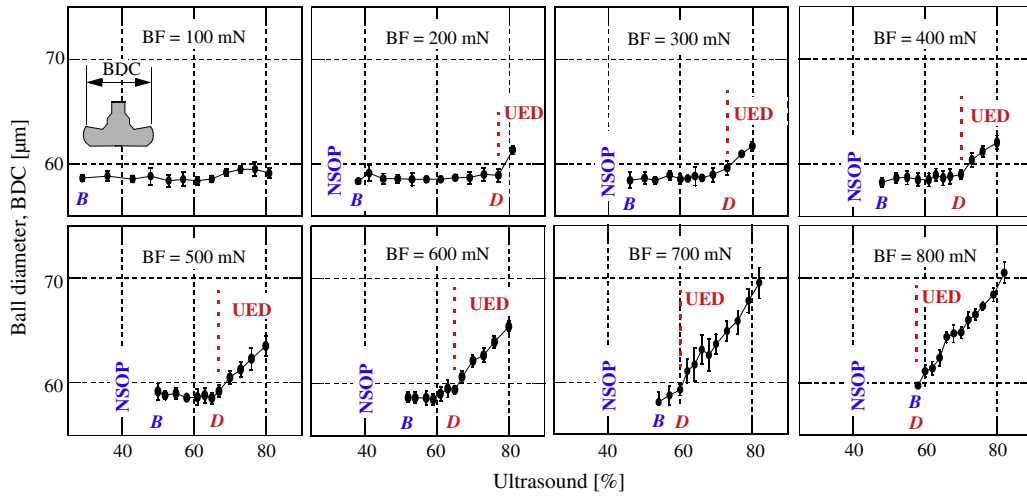
Fig. 4. Ball diameter (BDC) for different levels of US and BF. The NSOP and UED regions are shown.
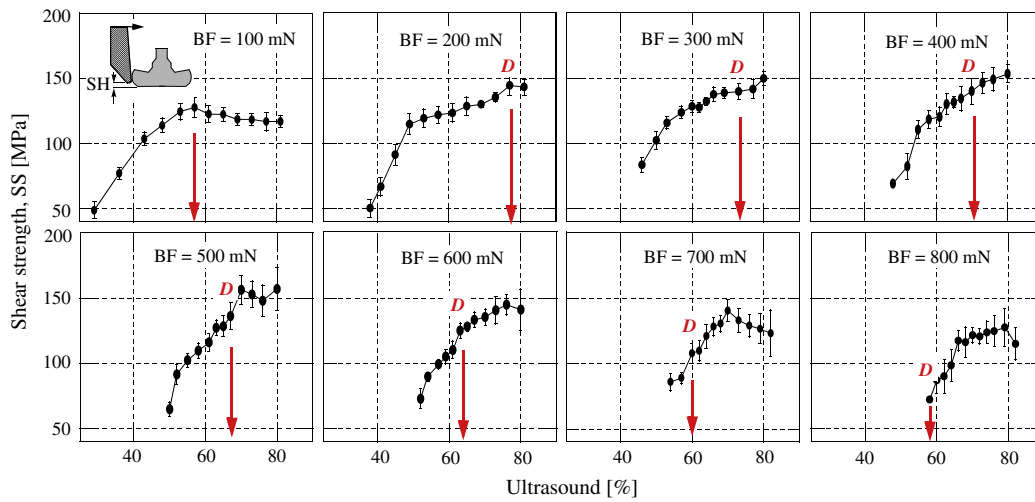

Fig. 5. Shear strength for different levels of US and BF. Arrows indicate optimum US level.

Table 2
Values of B and D for different levels of BF.

	Bond force [mN]							
	100	200	300	400	500	600	700	800
B [%]	29	38	46	48	50	52	54	58
D [%]	81	77	73	70	67	65	60	58

bonded ball circumference by, e.g., more than 10% as shown by its elliptical shape in Fig. 9b. The minor axis of the ellipse is in the US direction and the major axis is perpendicular to the US direction.

The amount of splash can be quantified using the SDI. The SDI value increases with increasing US and can be compared to the volume of pad wear W defined by the sliding wear model [36]
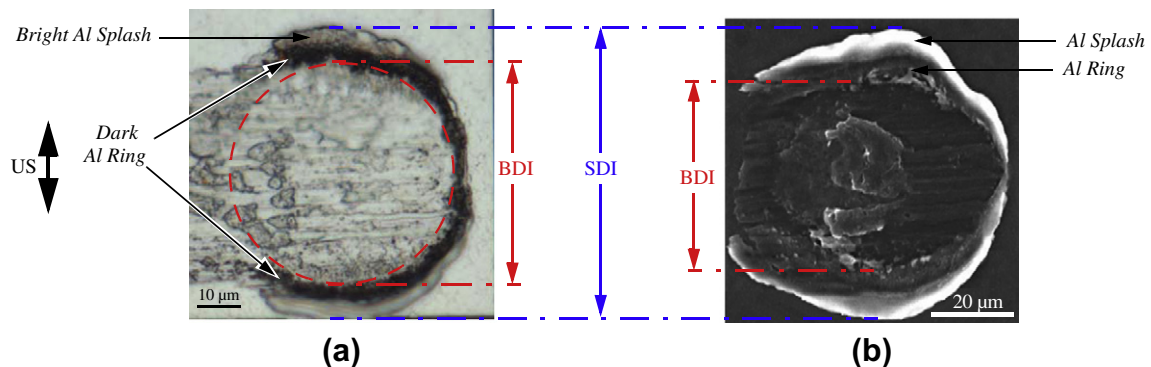

Fig. 6. (a) Optical and (b) SEM micrographs of typical sheared Cu ball bonds. Definitions of ball diameter at interface (BDI) and splash diameter at interface (SDI) are shown.
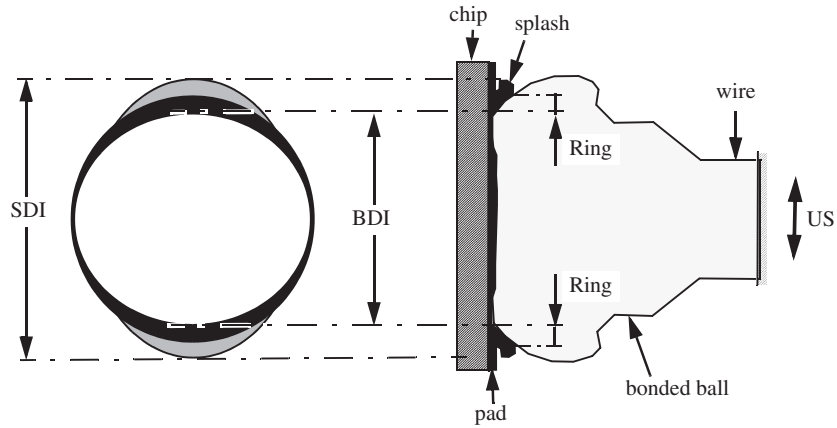
Fig. 7. Illustration of concave shaped ball/pad interface [34] due to "noodle effect" in Cu ball bonding. Optically bright and dark areas of splash are shown.
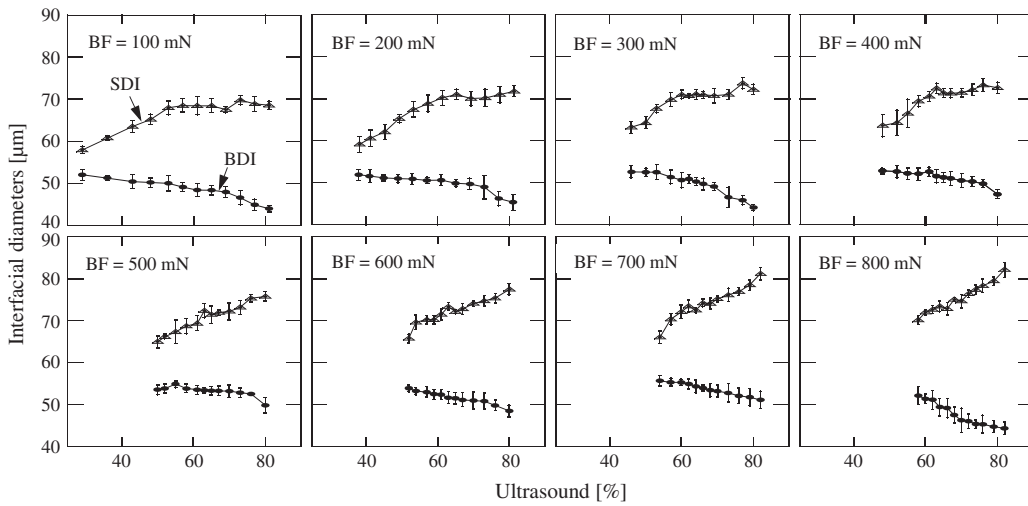

Fig. 8. Interfacial diameters: BDI (●) and SDI (△) for different levels of US and BF.
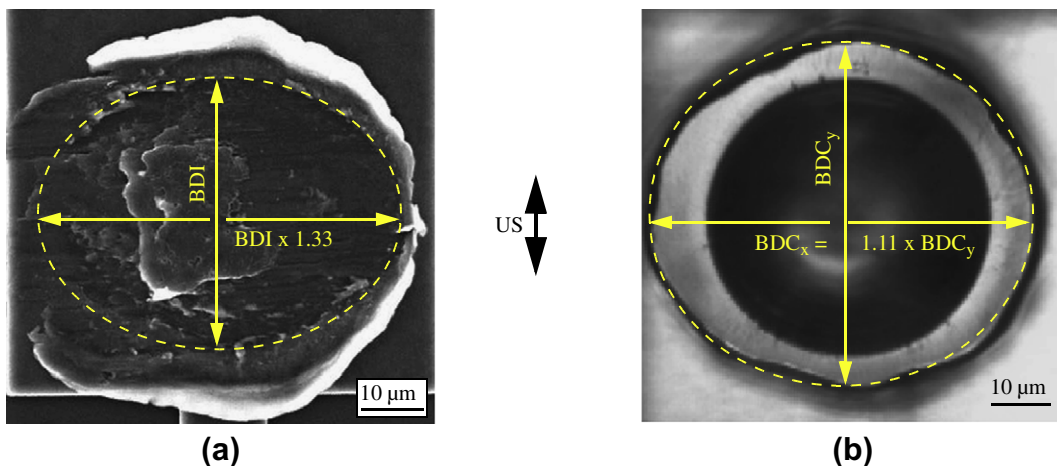

Fig. 9. Typical Cu ball bond (US = 77% and BF = 600 mN) with one of the smallest BDI: (a) SEM fractograph after shear; (b) optical micrograph of the bond before shear showing non-circular BDC. BDC = (BDC$_x$ + BDC$_y$)/2.

$$W = \frac{kLS}{3h} \qquad (1)$$

where k is the dimensionless wear coefficient, L is the normal load (BF in N), S is the sliding distance (in m), and h is the hardness of the softer material (in Pa), in this case the Al bond pad. According to Eq. (1), the higher the BF, the larger the SDI value. On the other hand, high US levels lead to larger sliding amplitudes, longer sliding distances for the same time, and to larger SDI values. These predictions are consistent with the experimental results observed in Fig. 8.

2.3. Maximum US force

A signal proportional to the shear stress induced to the bonding pad during bonding (US pad stress) is sensed using piezoresistive microsensors [10,11] integrated next to the bonding pad (Chip B). The microsensor type is described in [10,11]. It is calibrated to measure the *in situ* US tangential force F_{US} acting in the tangential direction on the bond pad during the bonding process, resulting in a sensitivity of $f = 17.2 \pm 0.9$ mV/V/N [11]. The US force is derived using $F_{US} = M/f$, where M is the non-dimensional response of the microsensor expressed in mV/V.

Ball bonding is performed on the microsensor test pad (Chip B) at the optimum US level and the US level needed to obtain shear strengths of ≈ 120 MPa (reduced US level) for different levels of BF. A baseline level of 120 MPa is selected since it is a typical shear strength achieved for a standard Au ball bonding process [10,11]. The values of the optimum US and the reduced US parameters for each BF level are taken from the process optimization conducted on Chip A, and shown in Table 3. The results are assumed to be valid for Chip B because of similar pad metallization on both chips. The measurements are performed on 10 chips. An example bond on the octagonal shaped bond pad of the microsensor is shown by the SEM micrograph in Fig. 10.

A typical microsensor signal and its fundamental amplitude is shown in Fig. 11a and b, respectively. The maximum US force induced to the bonding pad is evaluated at the point F_{max} shown in Fig. 11b. The value of F_{max} measured for optimum and reduced US levels for different levels of BF are plotted in Fig. 12. It is observed that for optimum US, a high BF level (BF = 600 mN, US = 65%) leads to $\approx 18\%$ reduction in the value of F_{max} than for low BF (BF = 200 mN, US = 77%). However, the value of SS drops from 144 MPa to 130 MPa for BF increasing from 200 mN to 600 mN. By using a lower value of BF (200 mN) combined with a reduced US level (US = 53%), the value of F_{max} can be reduced by $\approx 30\%$ (relative) while maintaining a SS of 120 MPa.

The optimum US level is the US level at which maximum SS is achieved for the targeted bonded ball geometry. For any given value of BF, the higher the US setting, the larger is the interfacial sliding. The interfacial sliding facilitates cleaning of the native oxides away from the interface, which is accompanied by the formation of micro-welds between the clean metal layers of the ball and the pad. The larger amount of interfacial sliding might possibly result in a larger number of micro-welds at the interface, resulting in a higher SS value. For the low BF levels, it is found that the maxi-
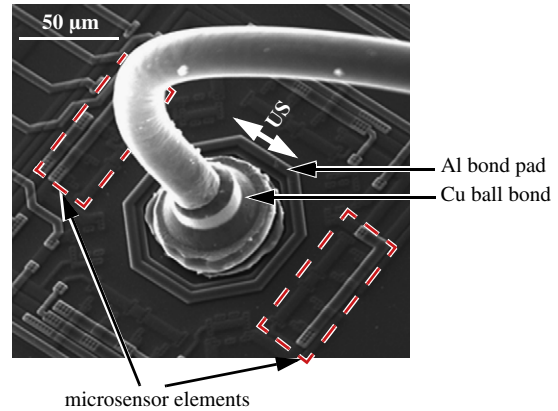

Fig. 10. SEM micrograph of a typical Cu ball bond (US = 70% and Bf = 400 mN) on microsensor test pad (chip B).
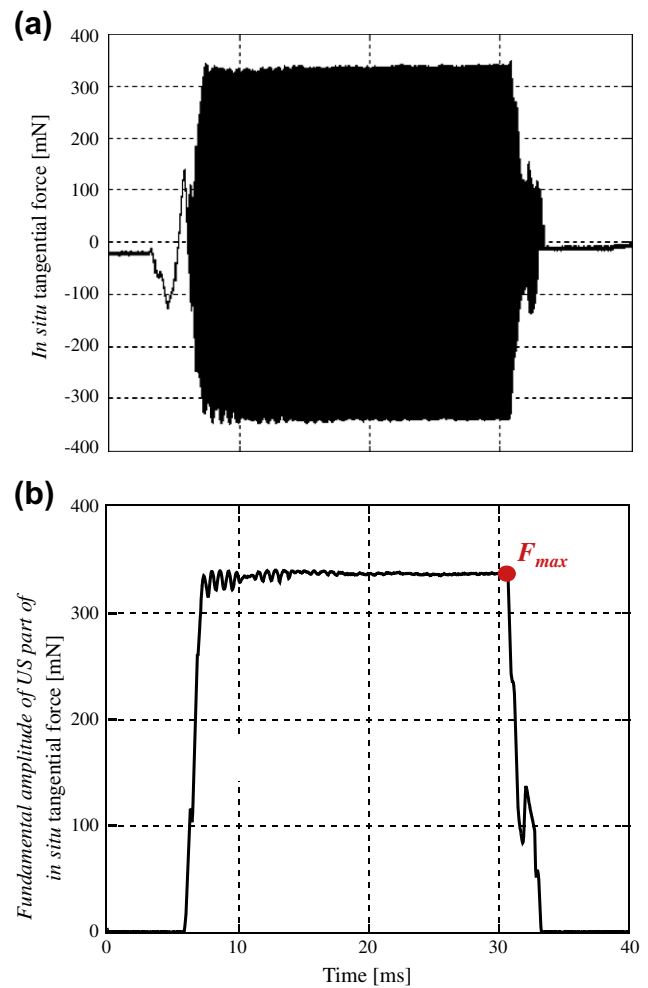

Fig. 11. Typical ultrasonic tangential force signal measured by the microsensor for BF = 200 mN and US = 78%. (a) Signal as measured; (b) signal conditioned for its fundamental amplitudes.

mum SS is achieved at a higher US setting (Fig. 5) while keeping the bond geometry within the target specifications. Note that the total pad stress is the superposition of the US caused stress to the BF caused stress. Since the F_{max} value is proportional to the US caused stress only, the higher values of the optimum US setting at the low BF levels result in the higher values of F_{max}. In contrast,
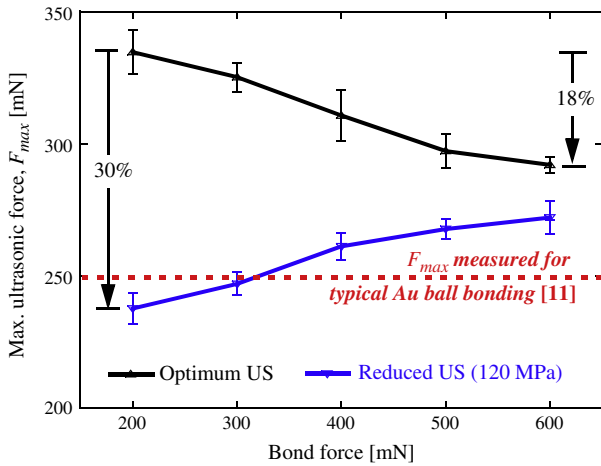
Table 3
Optimum and reduced US processes.

BF [mN]	Optimum		Reduced	
	SS [MPa]	US [%]	SS [MPa]	US [%]
200	144	77	≈ 120	53
300	140	73		55
400	140	70		58
500	136	67		60
600	130	65		62

Fig. 12. Maximum force acting on the pad (F_{max}) vs. bond force. The error bars indicate average ± standard deviation. The values of the US parameters used for optimum US and reduced US for each BF level are taken from Table 3.

for the reduced US process, the US level is selected at a constant SS of 120 MPa. A low BF value requires a low US level to start sliding (friction) at the interface. The lower US levels also cause lower amount of interfacial sliding, which might possibly result in a lower SS value, too. However, the bonding time (US period) used here is quite large, which possibly compensates for the low US levels by causing an equivalent amount of sliding required to obtain a SS of 120 MPa. For shorter bond times, the results might possibly be very different, which can be investigated in future studies.

2.4. Process window

The maximum US pad stress τ_{max} can be derived from F_{max} using

$$\tau_{max} = \frac{F_{max}}{S_i} \qquad (2)$$

where S_i is the nominal area of the elliptical bond interface. It is derived using

$$S_i = \frac{\pi \cdot BDI_x \cdot BDI_y}{4} \qquad (3)$$

where BDI_x and BDI_y are the major and minor diameters of the ellipse as shown in Fig. 9a.

Fig. 13 shows process results summarized in the US/BF space. The lines of friction and UED determined for Cu ball bonding process are shaped similar to those found for an Au process [35]. For any combination of US and BF which lies in the region below the line of friction, ball NSOPs are expected. Similarly, any combination of US and BF which lies above the line of deformation results in BDC values greater than 58 μm. Contour curves visualize the results for SS_I (SS at the interface) and τ_{max}, where $SS_I = SF/S_i$.

There is a trade-off between maximizing SS_I and controlling ball deformation. While staying below the deformation curve, SS_I reaches 180 MPa in region C shown in Fig. 13, and a conventional process window could be chosen within this region. However, this region also results in high values of τ_{max}, increasing the chances of pad damage. To minimize the chances of pad damage, Cu ball bonds can be made using parameter combinations lying in the lower stress bonding region R shown in Fig. 13. Within the region R, $SS_I \geqslant 140$ MPa and $\tau_{max} \leqslant 120$ MPa. These values of SS_I and τ_{max} correspond to those obtained for a typical Au ball bonding process [10,11]. Thus, by a thorough optimization of BF and US, it is possi-

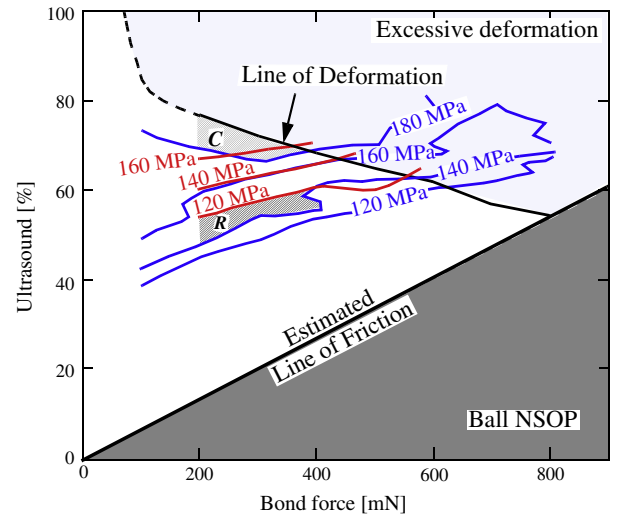**Fig. 13.** US/BF process space with window for low-stress Cu ball bonding (R). Blue and red contours are SS_I and τ_{max} contour lines, respectively. (For interpretation of the references to colour in this figure legend, the reader is referred to the web version of this article.)
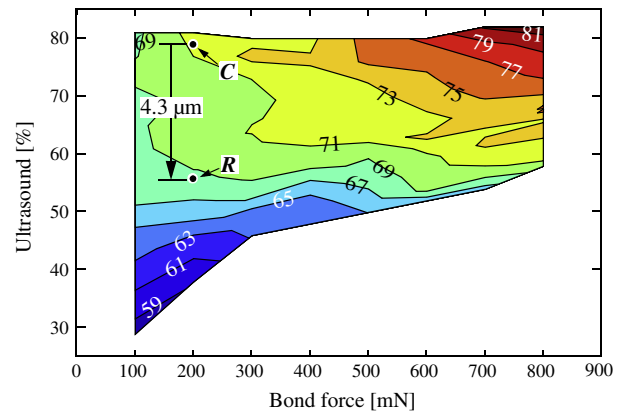

Fig. 14. Contour curves of SDI [μm] in US/BF space.

ble to completely eliminate the stress gap between Cu and Au ball bonding.

Fig. 14 shows the contour plot of SDI in the US/BF space. While the low-stress bonding region (R in Fig. 13) results in lower values of SDI, no universal correlation between SDI and F_{max} is observed. A possible reason for this might be that F_{max} quantifies the maximum average stress acting at the bond pad, but not the peak values. The localized peak stresses might be more influential in determining splash and pad failure. A detailed understanding of the effective underpad stress distribution would be helpful in gaining insights into pad failure mechanisms.

3. Conclusions

The conventional optimization aims at maximum bond shear strength for the targeted bond geometry. However, it also causes the highest ultrasonic stress on the pad. Therefore, a better optimization criterion could be adequately high shear strength, opposed to maximum shear strength. To this end, contour curves of the maximum ultrasonic force measured by the microsensor are shown in the US/BF process space. The results demonstrate that the underpad

damage risks typical to a Cu ball bonding process can be reduced by a thorough optimization of the bonding process settings for ultrasound and bond force. The amount of Al pad splash can also be reduced to a certain extent, however, it cannot be eliminated completely by controlling the ultrasound and bond force settings alone. Future work involves characterizing the long-term reliability performance of Cu ball bonds made with different parameter combinations.

Acknowledgements

References

[1] Greig WJ. Integrated circuit packaging, assembly and interconnections. Springer Science + Business Media; 2007.
[2] Harman G. Wire bonding in microelectronics materials, processes, reliability, and yield. 2nd ed. New York: McCraw-Hill; 1997.
[3] Zhou Y. Microjoining and nanojoining. Cambridge (England): Woodhead Publishing Ltd.; 2008.
[4] Assembly and packaging. In: Int tech roadmap for semicond; 2006. p. 1–19.
[5] Nguyen LT, McDonald D, Danker AR, Ng P. Optimization of copper wire bonding on Al–Cu metallization. IEEE Trans Compon Packag Manuf Technol 1995;18(2):423–9.
[6] Kaimori S, Nonaka T, Mizoguchi A. The development of Cu bonding wire with oxidation-resistant metal coating. IEEE Trans Adv Packag 2006;29(2):227–31.
[7] Srikanth N, Murali S, Hong YM, Vath CJ. Critical study of thermosonic copper ball bonding. Thin Solid Films 2004;462–463:339–45.
[8] Deley M, Levine L. The emergence of high volume copper ball bonding. In: Proc SEMICON west conf; 2004.
[9] Tan CW, Daud AR. Cratering on thermosonic copper wire ball bonding. J Mater Eng Perform 2002;11(3):283–7.
[10] Shah A, Mayer M, Zhou Y, Hong SJ. In-situ ultrasonic force signals during low temperature thermosonic copper wire bonding using piezo-resistive microsensors. Microelectron Eng 2008;85(9):1851–7.
[11] Shah A, Mayer M, Zhou Y, Hong SJ, Moon JT. Low-stress thermosonic copper ball bonding. IEEE Trans Electron Packag Manuf 2009;32(3).
[12] Tan CM, Er E, Hua Y, Chai V. Failure analysis of bond pad metal peeling using FIB and AFM. IEEE Trans Compon Packag Manuf Technol 1998;21(4):585–91.
[13] Tan CM, Linggajaya K, Er E, Chai V. Effect of BOE etching time on wire bonding quality. IEEE Trans Compon Packag Technol 1999;22(4):551–7.
[14] Tan CW, Daud AR. Bond pad cratering study by reliability tests. J Mater Sci: Mater Electron 2002;13(5):309–14.
[15] Caers J, Bischoff A, Falk J, Roggen J. Conditions for reliable ball/wedge copper wire bonding. In: Proc IEEE/CHMT Eur int electron man tech symp; 1993. p. 312–5.
[16] Ho HM, Tan YC, Tan WC, Goh HM. Investigation of factors affecting bonded ball hardness on copper wire bonding. In: Proc IMAPS conf on microelectron packag, Taiwan; 2006.
[17] Wulff FW, Breach CD, Stephan D, Saraswati Dittmet KJ. Characterisation of intermetallic growth in copper and gold ball bonds on aluminum metalliation. In: Proc IEEE electron packag tech conf; 2004.
[18] Wulff FW, Breach CD, Stephan D, Saraswati Dittmet KJ, Garnier M. Further characterisation of intermetallic growth in copper and gold ball bonds on aluminum metalliation. In: Proc SEMI tech symp; 2005.
[19] Hang CJ, Wang CQ, Mayer M, Tian YH, Zhou Y, Wang HH. Growth behavior of Cu/Al intermetallic compounds and cracks in copper ball bonds during isothermal aging. J Microelectron Reliab 2008;48:416–24.
[20] Zhong ZW, Ho HM, Tan WC, Goh HM, Toh BH, Tan J. Study of factors affecting the hardness of ball bonds in Cu wire bonding. Microelectron Eng 2007;84:368–74.
[21] Onuki J, Koizumi M, Suzuki H. Influence of ball-forming conditions on the hardness of copper balls. J Appl Phys 1990;68(11):5610–4.
[22] Lum I, Huang H, Chang BH, Mayer M, Du D, Zhou Y. Effect of super-imposed ultrasound on the deformability of gold. J Appl Phys 2009;105(024905).
[23] Pequegnat A, Hang CJ, Mayer M, Zhou Y, Moon JT, Persic J. Effect of EFO parameters on Cu FAB hardness and work hardening in thermosonic wire bonding. J Mater Sci: Mater Electron 2009.
[24] McKenna RG, Mahle RL. High impact bonding to improve reliability of VLSI die in plastic packages. In: Proc IEEE electron comp conf; 1989. p. 424–7.
[25] Toyozawa K, Fujita K, Minamide S, Maeda T. Development of copper wire bonding application technology. IEEE Trans Compon Hybr Manuf Technol 1990;13(4):667–72.
[26] Liu Y, Irving S, Luk T. Thermosonic wire bonding process simulation and bond pad over active stress analysis. IEEE Trans Electron Packag Manuf 2008;31(1):61–71.
[27] Chylak B, Ling J, Clauberg H, Thieme T. Next generation nickel-based bond pads enable copper wire bonding. ECS Trans 2009;18(1):777–85.
[28] Qin I, Shah A, Huynh C, Meyer M, Mayer M, Zhou Y. Effect of process parameters on pad damage during Au and Cu ball bonding processes. In: Proc IEEE electron packag tech conf; 2009. p. 573–8.
[29] Shah A, Mayer M, Zhou Y, Moon JT, Persic J. Optimization of ultrasound and bond force to reduce pad stress in thermosonic Cu ball bonding. In: Proc IEEE electron packag tech conf; 2009. p. 10–15.
[30] Mayer M, Paul O, Bolliger D, Baltes H. In-situ calibration of wire bonder ultrasonic system using integrated microsensor. In: Proc IEEE electron packag tech conf; 1998. p. 219–23.
[31] Lee J, Mayer M, Zhou Y, Hong SJ. Iterative optimization of tail breaking force of 1 mil wire thermosonic ball bonding processes and the influence of plasma cleaning. Microelectron J 2007;38:842–7.
[32] Schwizer J, Mayer M, Brand O. Force sensors for microelectronic packaging applications. New York: Springer Science, Series: Microtechnology and MEMS; 2005.
[33] Gaul H, Schneider-Ramelow M, Lang K-D, Reichl H. Predicting the shear strength of a wire bond using laser vibration measurements. In: Proc of the 1st electron systemintegration tech conf, vol. 2; 2006. p. 719–25.
[34] Qin I, Shah A, Cuong H, Meyer M, Mayer M, Zhou Y. Effect of process parameters on pad stress during Au and Cu ball bonding processes. In: Proc of 11th IEEE electron packag and tech conf; 2009. p. 573–8.
[35] Mayer M, Schwizer J. Thermosonic ball bonding model based on ultrasonic friction power. In: Proc IEEE electron packag tech conf; 2003. p. 738–43.
[36] Archard JF. Contact and rubbing of flat surfaces. J Appl Phys 1953;24:981–8.